FINAL DRAFT

CONF-810434--2(Draft)

MEASUREMENT OF TRANSIENT TWO-PHASE FLOW VELOCITY USING STATISTICAL SIGNAL ANALYSIS OF IMPEDANCE PROBE SIGNALS

W. H. Leavell, J. A. Mullens
Instrumentation and Controls Division
Oak Ridge National Laboratory
Oak Ridge, TN 37830

Sponsored by the U.S. Nuclear Regulatory Commission, Office of Nuclear Regulatory Research under Interagency Agreements DOE 40-551-75 and 40-552-75 NRC FIN No. B0413 with the U.S. Department of Energy under contract W-7405-eng-26 with the Union Carbide Corporation

Abstract

A computational algorithm has been developed to measure transient, phase-interface velocity in two-phase, steam-water systems. The algorithm developed under the sponsorship of the U.S. Nuclear Regulatory Commission's Office of Nuclear Regulatory Research will be used to measure the transient velocity of steam-water mixture during simulated PWR reflood experiments. By utilizing signals produced by two, spatially separated impedance probes immersed in a two-phase mixture, the algorithm computes the average transit time of mixture fluctuations moving between the two probes. This transit time is computed by first, measuring the phase shift between the two probe signals after transformation to the frequency domain and then computing the phase shift slope by a weighted least-squares fitting technique. Our algorithm, which has been tested with both simulated and real data, is able to accurately track velocity transients as fast as 4 m/sec/sec.

I. Introduction

A computational algorithm has been developed to measure transient, phase-interface velocity in two-phase, steam-water systems by utilizing signals produced by two, spatially-separated impedance probes. The phase-interface velocity computed by the algorithm will be used to aid in the interpretation of mass transport prediction made by newly developed thermohydralic models[1] for simulated PWR reflood experiments. These models assume that the transient dynamics of each phase of a two-phase mixture can be estimated by their own set of conservation equations and interphase transfer relationships[1].

The algorithm which measures the transit time of mixture fluctuation moving between two spatially-separated probes extends well-established, steady-state signal analysis methods[2] to handle transient data through the use of short-time averaging and overlap-processing techniques and a weighted, linear-least-squares phase fitting technique in the frequency domain. Cross-correlation analysis of signals from various types of probes has been successfully used in the past to compute transit time data mainly for steady-state, two-phase flow and attempts to extend this technique to transient two-phase flow have also been done with some success[4-8]. Our algorithm by operating on the probe signals in the frequency domain has overcome some of the limitations of time-domain, cross-correlation analysis.

II. Probe Signals

The probes used in this application measure the electrical impedance of each fluid phase (the vapor phase has a high impedance whereas the

liquid phase has a low impedance)[9]. Figure 1 shows typical signals from a pair of impedance probe's detecting water droplets in steam. The figure illustrates the apparently random nature of the signals and the fact that the flow produces a somewhat different signal at each probe.

III. Transit Time Calculation Methods

There are two different methods for computing the transit time or time delay between two random signals. The first method operates on the two signals in the time domain and is known as the cross-correlation method[2]. The second method operates on the two signals in the frequency domain and is known as the cross-power spectral density method[2]. The two methods are related by the Fourier transform. The cross-correlation function of two random time signals x(t) and y(t) is defined as:

$$R_{xy}(\tau) = \lim_{T\to\infty} \frac{1}{T}\int_0^T x(t)y(t+\tau)dt \qquad (1)$$

where τ is the time delay variable and T is the integration time. The function $R_{xy}(\tau)$ will have a maximum value for some particular time delay τ_0 that is equal to the transit time of the phase-interface.

In the frequency domain, the cross power-spectral density (CPSD) function of x(t) and y(t) can be defined two ways:

$$\Phi_{xy} = \mathcal{F}[R_{xy}(\tau)] = \mathcal{F}[x(t)]\,\mathcal{F}^*[y(t)] \qquad (2)$$

where $\mathcal{F}[\ ]$ denotes the Fourier transform and $\mathcal{F}^*[\ ]$ denotes the complex conjugate of the Fourier transform.

The CPSD function can also be represented in polar form as:

$$\Phi_{xy}(f) = M(f)e^{-j\theta(f)} \tag{3}$$

where M(f) is the magnitude and $\theta(f)$ is the phase. For a process characterized by a simple transport delay $\theta(f)$ is a linear function of frequency with an intercept value of 0° at 0 Hz. The slope of the phase curve is related to the transport delay, τ_o, by:

$$\tau_o = \frac{1}{360}\frac{d\theta(f)}{df} \tag{4}$$

Accordingly, to estimate the slope of $\theta(f)$, a straight line passing through 0° at 0 Hz can be fitted to the phase estimates obtained at various frequencies. However, a fit using all the phase extimates often does not work satisfactorily, due to phase errors introduced by process and measurement noise.

If the process is stationary, both $R_{xy}(\tau)$ and $\Phi_{xy}(f)$ can be averaged over long intervals of time to reduce statistical variance and effects of additive incoherent noise[2]. However, if the process is non-stationary or transient, long time averages will introduce error in the estimation of transport time, since the transport time will vary throughout the measurement time period[2].

Since short-time averages are required to track a changing transport time, another means for reducing the phase variance produced by incoherent noise must be sought. One such technique[2] uses the coherence function to

identify the frequency range over which the true process signal dominates and thus to restrict the analysis to that frequency range for which the signal-to-noise ratio is high.

A measure of the noise contamination can be computed using the coherence function of the two probe signals[2]. The coherence function, $\gamma^2(f)$, takes on values between 0 and 1, 0 indicating the presence of incoherent noise only and 1 indicating uncontaminated signal. This function is defined as:

$$\gamma^2(f) = \frac{|\Phi_{xy}(f)|^2}{\Phi_{xx}(f)\,\Phi_{yy}(f)} \qquad (5)$$

where Φ_{xy} and Φ_{xx}, Φ_{yy} are the cross- and auto-power spectral density functions of the two probe signals, x(t) and y(t). The coherence function is used to identify the frequency range over which there is the smallest amount of noise contamination.. We have used the coherence estimates to weight the linear fit of the CPSD phase estimates vs. frequency to discriminate against noise.

IV. Computational Algorithm

A computational algorithm has been developed based on the frequency domain technique outlined above. The algorithm has three basic parts: (1) estimation of short-time averaged CPSD, PSD, and coherence functions; (2) computation and tracking of the CPSD phase estimates; and (3) estimation of the CPSD phase slope by a coherence-weighted linear fitting technique

IVa. Short-Time Averaged Spectral Estimates

The first part of the algorithm produces 1-s averages of the two probe signals' coherence function, and the auto- and cross-power spectral

density functions. One second of data (512 samples) from each probe signal constitutes an analysis interval. These analysis intervals are further partitioned into 64-point blocks, which are overlapped in time by one-half their length to produce a total of 15 blocks of signal data for each probe signal for each second of elapsed time. Each data block is weighted with a Hanning weighting function and then transformed using a fast Fourier transform algorithm. The resulting 32 transformed values are operated on as follows to produce spectral estimates:

$$\hat{\Phi}_{xx}(f) = X(f)\,X^{*}(f) \tag{6}$$

$$\hat{\Phi}_{yy}(f) = Y(f)\,Y^{*}(f) \tag{7}$$

$$\hat{\Phi}_{xy}(f) = X(f)\,Y^{*}(f) \tag{8}$$

Here X(f) = F[x(t)] and Y(f) = F[y(t)] . The 15 estimates (one for each overlapped block) of $\hat{\Phi}_{xx}$, $\hat{\Phi}_{yy}$, and $\hat{\Phi}_{xy}$ for each 64 point data block are then averaged together to produce 1-s averaged values for the spectral density functions. The average coherence function for this same one second of data is then calculated from the averaged spectral density functions as:

$$\gamma^2(f) = \frac{\left| \overline{\Phi_{xy}(f)} \right|^2}{\overline{\Phi_{xx}(f)}\,\overline{\Phi_{yy}(f)}} \tag{9}$$

IVb. Phase Calculation and Tracking

The second part of the algorithm involves the calculation of the phase estimates using the 32 real and imaginary pairs of the CPSD estimates. The phase angles are defined as:

$$\theta(f) = \tan^{-1} \frac{Im\left[\overline{\Phi_{xy}(f)}\right]}{Re\left[\overline{\Phi_{xy}(f)}\right]} \tag{10}$$

This step produces angles between ± 180° since the inverse tangent function is multiple valued. In order to produce a single-valued phase function, which is required for slope estimation, a second operation, phase tracking, is performed on the phase estimates to eliminate the artificial periodicity produced by the inverse tangent calculation. Our method of tracking uses an iterative procedure in which an initial slope is first estimated using the lowest frequency, phase estimate. The initial slope so derived is used to project a value for the next phase estimate. A comparison is then made between the projected value and the actual value of the next phase estimate. If the difference is greater than ± 180°, a 360° correction is made to the value given by Eq. (10). This corrected phase estimate is again compared to the projected value and is corrected again if the difference is still greater than ± 180°, Corrections and comparisons are continued until the difference is less than ± 180°, at which point the corrected phase estimate is used to update

the previous slope estimate. The revised slope estimate, in turn, is used to project the next phase estimate. This iterative process is repeated until all 32 estimates have been examined and corrected to produce a single-valued phase function at each frequency.

IVc. Phase Slope Estimation

The final step in the algorithm is the estimation of the corrected phase function's slope. This is done by fitting a straight line passing through 0° at 0 Hz to the phase estimates, corrected as described above, using a conventional linear-least-squares procedure (see Appendix A) with coherence weighting. The slope of the least-squares line is:

$$\frac{d\theta(f)}{df} = \frac{\sum_{i}^{N} \gamma^2(f_i)\theta(f_i)f_i}{\sum_{i}^{N} \gamma^2(f_i)f_i^2} \qquad (11)$$

where

$\gamma^2(f_i)$ = coherence estimate at frequency f_i

N = total number of phase estimates

The best estimate of transport delay is then computed by Eq. (4).

The frequency range over which the phase function is linear has been found to be a function of the flow regime of two-phase, steam-water mixtures tested for this application. For a high-velocity, droplet-flow regime, the phase will typically be linear up to 400-500 Hz while for a low-velocity, slug-flow regime, the phase may only be linear up to 100 Hz. Since many different flow regimes are likely to be present throughout the duration of a reflood transient, the frequency range over which the phase is linear will thereby be a variable. In the majority

of cases studied by the authors, the phase is reasonably linear up to $\sim$ 100 Hz for the impedance probes used in this application, so our practice has been to restrict the least-squares fit to the range 0-100 Hz.

IVd. Transport Delay Error Estimation

To quantify the likely range of values that a transport time estimate may have for a given analysis time interval, an error estimate was computed that compares the estimated transport time to all possible transport times for the given time interval. To establish the set of all possible transport times, a line passing through 0° at 0 Hz is projected to each individual phase estimate and the slope of that line is used to calculate one transport time. A standard deviation is then computed between the set of all possible transport times and that computed by the weighted fit described above. This standard deviation is the error estimate used in all the succeeding algorithm tests.

Although the recommended algorithm is more complicated than a straight-forward cross-correlation calculation, it often succeeds where the simpler analysis fails, since it provides an adaptive optimization of the signal-to-noise ratio by using the coherence estimates to emphasize the true signal effects in relation to contaminating noise.

V. Algorithm Tests

Va. Simulated Data

In order to demonstrate that the algorithm computes the time delay correctly, a computer program (see Appendix B) was written to simulate probe signals for known conditions. The program was designed to simulate

both steady-state and transient transport delay and includes options to vary both the signal-to-noise ratio and the number and size of random detection events occurring in a given time interval. Figure 2 is an example of a simulated probe signal for a 250 ms. time interval.

In a test of the inherent accuracy of the algorithm, five 400-s data sets were generated with constant time delays of 1, 3, 5, 7 and 9 ms. No noise contamination was added so that calculation biases (if any) would be readily identifiable. Each 400-s data set was subdivided into 1-s intervals of 512 points, and each such interval was analyzed to produce estimates of the time delay. The average and standard deviation of the 1-s time delay estimates is given in Table 1, along with the true time delay. In each case in Table 1 the maximum error between the true and calculated delay was less than 2% of value, and the standard deviation of calculated delay was less than 1% of its mean value. Although no contaminating noise was present, the randomness of event generation made the signals' coherence range between values of 0.93 and 0.99. The presence of any noise, no matter how small, tends to cause the algorithm to slightly underestimate the true delay (see Table 1). This is thought to be due to the noise biasing the phase estimates toward 0°, thus producing a smaller phase slope and, consequently, a shorter time delay. To further investigate the effects of noise on the measured time delay, nine data sets were generated with nine different average coherences ranging in value from 0.98 to 0.11.

Figure 3 shows the resulting average time delays plotted versus coherence. In each case the average delay is slightly less than the

true delay, and the variance of the computed delay increases rapidly for coherence values < 0.3.

To test the transient tracking capability, three data sets were generated in which the velocity was decreased linearly from 20 to 2 m/s over three different time intervals (5, 20, and 80 s). For a simulated 20 mm probe spacing, the transport time was found to vary inversely with velocity (from 1 to 10 ms) as expected. The analysis results consisted of 1-s averages of the transport delay. Figure 4 shows the calculated delay vs. time for the three transients. The average signal coherence for these transients was $\sim$ 0.7. In all three cases the transients were accurately tracked by the algorithm. The last estimate of delay in each case was < 10 ms due to the rapid change in transport delay during the last second of data.

In order to determine the effects of contaminating noise on the transient delay calculations, three transient cases were generated in which broadband noise was added to the simulated signals to produce coherences of 0.8, 0.5 and 0.3. For each case the velocity decreased linearly from 20 m/s to 2 m/s over a 20 s time interval. Figs 5-7 show the transport delay results vs. time. The algorithm reliably tracked the transient in all three cases. The effects of increasing noise seem to be most noticeable for transport delays < 2 ms. This is to be expected since the slope of the phase is small (< 1° Hz^{-1}) for such a short transport delay and small changes in the slope due to noise effects thereby produce larger changes in the computed transport delay than would result for longer delays.

To determine the effect of using averaging times < 1 s to compute transient delays, a 20 - 2 m/s transient case spanning a 5-s time interval was analyzed using 1, 0.5, and 0.25-s averaged delays. The results of the three analyses are shown in Figs. 8-10. Although the variance for each delay estimate increased as shorter time averages were used, the average computed delay still tracked the true delay.

Vb. Analysis of Real Transient Data

A series of tests[10] were conducted during which transient, steam-water flow was produced. The tests were designed to approximate the reflood stage of a PWR loss-of-coolant accident. A test bundle consisting of a 3x3 array of electrically-heated rods was used to simulate a reactor fuel bundle. One rod of the array was instrumented with two pairs of impedance probes which sensed the two-phase flow produced in a sub-channel of the rod array. The spacing between probes in each pair was ∿ 19 mm.

The test stages included a pre-heat of the rod bundle of 500° C at which time water was injected at a constant flow rate until the rod bundle was quenched. During each test the impedance probe signals were recorded on an analog tape recorder and high-speed photographs were made of two-phase flow occurring in the vicinity of one probe pair. Sequential frames from these photographs later gave an optically derived estimate of droplet velocity near the impedance probe which was compared to the value derived from the impedance probe measurements.

We analyzed the probe signals with our algorithm and obtained 1-s averages of the transport delay. During each transient the velocity varied from 5 - 0 m/s over time intervals of 300 to 400 s. Velocity could

be calculated from the onset of droplet flow until such time the probes became immersed by the rising water.

Figure 11 is an example of the velocities measured for one reflood transient. During the first 70-80 s only steam was present in the probe's sub-channel; at ∿ 80 s droplets were detected and the first velocity estimates could be made. The inferred velocity decreased slowly over the next 300 s until the probes were immersed by the water at ∿ 400 s. A plot (Fig. 12) of the estimated maximum and minimum values of the transport delay for each 1-s estimate of the transient shows the measurement uncertainty.

High-speed color xenon flash photographs were taken of the two-phase flow using a double exposure technique with red and green flashes. This technique[10] permitted the motion of many droplets to be obtained at once, from which an estimate of the average droplet size and velocity could be made. A simple comparison of the probe-inferred and photograph-inferred transport times is somewhat misleading since the former represent 1-s time-averaged values whereas the latter spatial averages at the instant of the photograph. However, such comparison is interesting, as shown in Fig. 13, where the transport delays inferred by the two methods are plotted vs. time. The photographic transport times tend to be smaller than the probe-inferred values in the majority of the cases.

At this time, the authors can not offer an adequate explanation of the discrepancy between the two methods except that the probes may tend to impede the larger droplets during sampling of the mixture.

VI. Current Work

The algorithm is currently being integrated into a larger data acquisition and analysis system that will be used to analyze recorded data produced by PWR reflood test facilities under construction in Germany and Japan. Further work on relating the measured phase interface velocity to the steam and water velocity is continuing.

VII. Summary

A computer algorithm was developed that will compute and track changes in two-phase flow velocity using as input signals from two spatially separated impedance probes. The transport delay is computed by estimating the slope of the phase shift between the two probe signals over short time intervals. The algorithm uses coherence function weighting to minimize effects of incoherent noise. Tests with simulated data show that the algorithm will track transient transport delays accurately. Tests with real data from a simulated reflood experiment likewise show that the algorithm provides transport delay estimates that are in reasonable agreement with values derived by other methods.

Acknowledgement

The authors would like to acknowledge J. E. Mott and F. Shahrokhi for their valuable assistance in the early development stages of the algorithm. We would also like to acknowledge J. E. Hardy, M. J. Roberts, and T. J. Paulus for their valuable assistance in acquiring the transient, two-phase, impedance-probe signals during the reflood tests, and H. Leibert for the aquisition and analysis of the high-speed photographs of the two-phase flow.

Appendix A

The Derivation of the Phase Slope Formula Using Coherence Weighted Linear Least-Squares Fit

Given the following:

$$\theta_i = \{\theta(f_i), i = 1 \text{ to } N\} \tag{A1}$$

and

$$\hat{\theta}_i = S f_i \,, \; i = 1 \text{ to } N \tag{A2}$$

we define a weighted mean square error between Eqs. A1 and A2 as:

$$\overline{\epsilon^2} = \frac{1}{N} \sum_{i=1}^{N} W_i (\theta_i - S f_i)^2 \tag{A3}$$

expanding Eq. (A3) yields

$$\overline{\epsilon^2} = \frac{1}{N} \sum_{i=1}^{N} W_i (\theta_i^2 - 2\theta_i S f_i + S^2 f_i^2) \tag{A4}$$

To find $\overline{\epsilon^2}$ minimum, we take the partial derivative of Eq(A4) with respect to S which yields:

$$\frac{\partial \overline{\epsilon^2}}{\partial S} = \frac{1}{N} \sum_{i=1}^{N} W_i (-2\theta_i f_i + 2 S f_i^2) \tag{A5}$$

and set Eq. A5 equal to 0 which yields:

$$0 = -2 \sum_{i=1}^{N} W_i \theta_i f_i + S \sum_{i=1}^{N} W_i f_i^2 \qquad \text{(A6)}$$

Solving for S in Eq A6 yields:

$$S = \frac{\sum_{i=1}^{N} W_i \theta_i f_i}{\sum_{i=1}^{N} W_i f_i^2} \qquad \text{(A7)}$$

where $W_i = \gamma^2(f_i)$, the signal coherence at frequency f_i and S is the slope.

Appendix B

Droplets, A Probe Signal Simulation Program

DRPLTS (DRoPLeTS) simulates the one-dimensional flow of droplets past two sensors. Even though the model of the sensor response to the droplets is simplified the simulations produced by DRPLTS are very similar to signals produced by real sensors. DRPLTS consists of two main sections, flow simulation and sensor simulation.

DRPLTS uses probability distributions and a random number generator to generate a flow. Three quantities are generated randomly for each droplet, (1) droplet length, (2) droplet velocity, and (3) time of appearance of the droplet. Transients are simulated by changing the probability distributions.

The sensor simulation is unconventional in that it does not use digital signal techniques even though the final output of DRPLTS is a digitized signal. Instead, the continuous (analog) differential equations are solved. The modeled sensor responds to the presence of a droplet in a binary fashion, with a measured void fraction of 0.0 if any part of the droplet is within the length of the sensor or 1.0 if not. If contaminating noise is present, the void fraction output is modified by a random number but the resulting void fraction still lies between 0.0 and 1.0. Because the signals are analyzed using digital signal processing techniques, the signal bandwidth must be limited. Real signals would be anti-abased via analog filters, and DRPLTS simulates two-pole analog filters precisely.

The digitized signal is produced by solving the differential equations for each instant of digitization.

Table 1

Calculated Transport Times

For Steady-State, Simulated Data

Simulated Transport Time (ms)	Average Algorithm Computed Transport Time and Standard Deviation (ms)
1.00	0.99 ± 0.06
3.00	2.97 ± 0.02
5.00	4.92 ± 0.03
7.00	6.89 ± 0.03
9.00	8.82 ± 0.04

References

1. L. J. Agee, "Multi-fluid Models for Transient Two-Phase Flow," Electric Power Research Institute, NP-618-SR, June, 1978.

2. J. S. Bendat, A. G. Piersol, Random Data: Analysis and Measurement Procedures, Wiley-Interscience, New York, 1971.

3. G. F. Hewitt, P. C. Lovegrove, "Experimental Methods in Two-Phase Flow Studies," Electric Power Research Institute, NP-118, July, 1976.

4. G. D. Lassahn, "Two-Phase Flow Velocity Measurement With Radiation Intensity Correlation," Aerojet Nuclear Co., ANCR-1216, July, 1975.

5. Keiji Miyazaki, et. al., "Measurement of Propagation Velocities of Pressure and Void by Cross-Correlation of Fluctuations in Nitrogen-Water Flow," Journal of Nuclear Science and Technology, V. 10, May, 1973.

6. S. T. Olszowski, J. Coulthard, and R. S. Sayles, "Measurement of Disperced Two-Phase Gas-Liquid Flow By Cross Correlation of Modulated Ultrasonic Signals," International Journal of Multiphase Flow, V. 2, Pergamon/Elsevier, Great Britain, 1976.

7, S. Banerjee, T. R. Heidrick, and J. R. Saltvold, "Measurement of Void Fraction and Mass Velocity In Transient Two-Phase Flow," Specialists Meeting On Transient Two-Phase Flow, Toronto, August 3-4, 1976.

8. A. C. Raptes, G. F. Popper, "The Analysis of Thermal Fluctuations In the Semiscale Tests To Determine Flow Transit Delay Times Using A Transfer Function Cross-Correlation Technique," ANL-CT-77-17, August, 1977.

9. B. G. Eads, et al, "Advanced Instrumentation for Reflood Studies Program Quarterly Progress Report, October 1-December 31, 1977," NUREG/CR-0213, ORNL/NUREG/TM-202, September, 1978.

10. W. H. Leavell, J. E. Hardy, H. Leibert, and J. A. Mullens, "Transient Testing of An In-Core Impedance Flow Sensor In A 9-Rod Heated Bundle," ORNL/NUREG/TM-389, (to be published).

Figure Captions

Fig. 1 An example of impedance probe signals for a steam-water mixture.

Fig. 2 An example of a simulated impedance probe signal.

Fig. 3 Transit time as a function of coherence calculated with simulated signals having a delay of 5 ms.

Fig. 4 Transit time versus time calculated for a 5, 20, and 80 s. simulated transient delay.

Fig. 5 Calculated transit time versus time for a 20 s simulated transient delay with a 0.8 average signal coherence.

Fig. 6 Calculated transit time versus time for a 20 s simulated transient delay with a 0.5 average signal coherence.

Fig. 7 Calculated transit time versus time for a 20 s simulated transient delay with a 0.3 average signal coherence.

Fig. 8 1-s averaged transit time versus time for a 5 s simulated transient delay.

Fig. 9 0.5-s averaged transit time versus time for a 5 s simulated transient delay.

Fig. 10 0.25 averaged transit time versus time for a 5 s. simulated transient delay.

Fig. 11 Phase interface velocity versus time for a real steam-water transient produced by a simulated reflood experiment.

Fig. 12 Maximum and minimum transport delay calculated for a real steam-water transient produced by a simulated reflood experiment.

Fig. 13 A comparison versus time of transport delay calculated by the algorithm (0) and by high-speed photographs (x) for a part of a real steam-water transient.

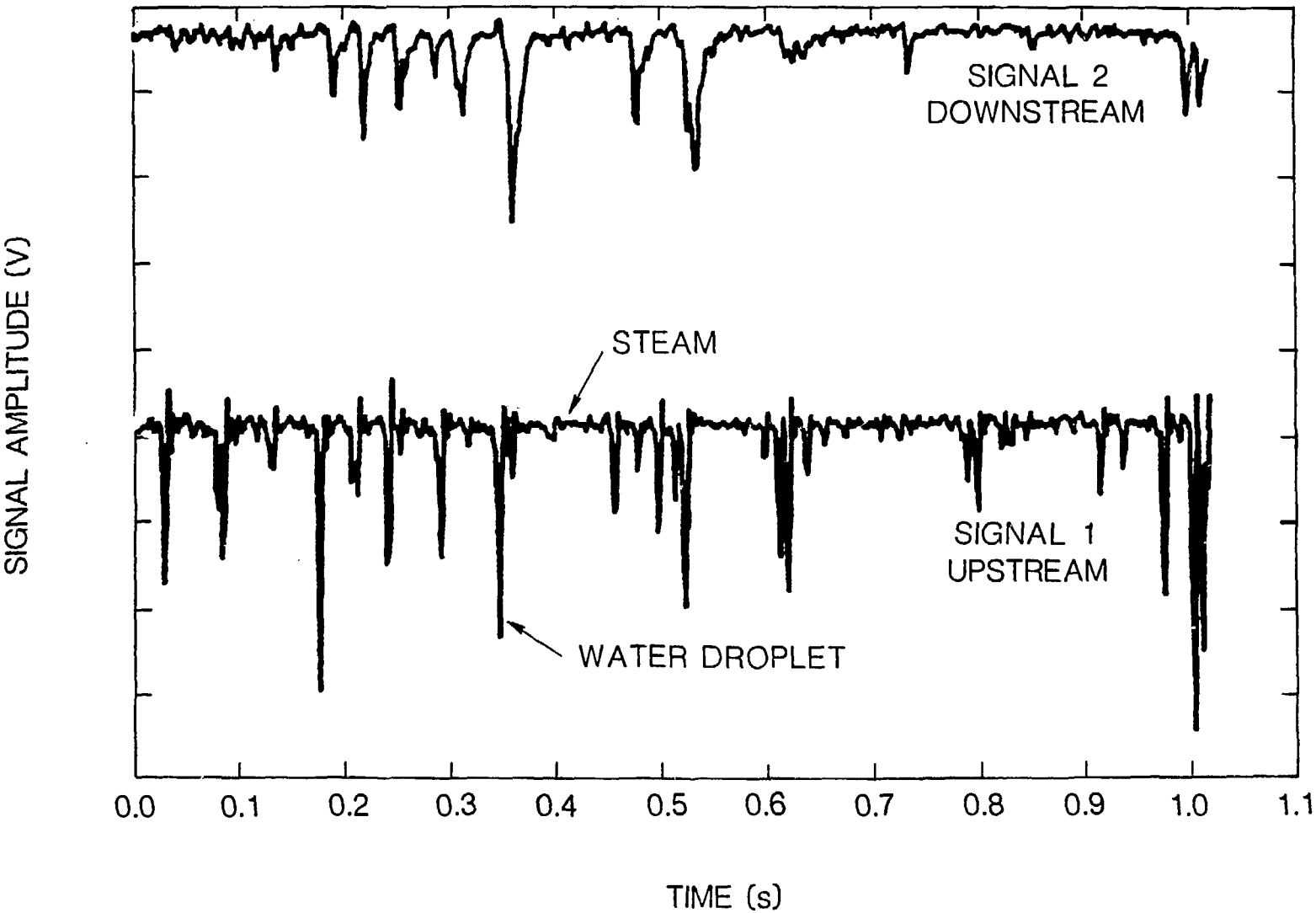

Fig. 1 An example of impedance probe signals for a steam-water mixture.

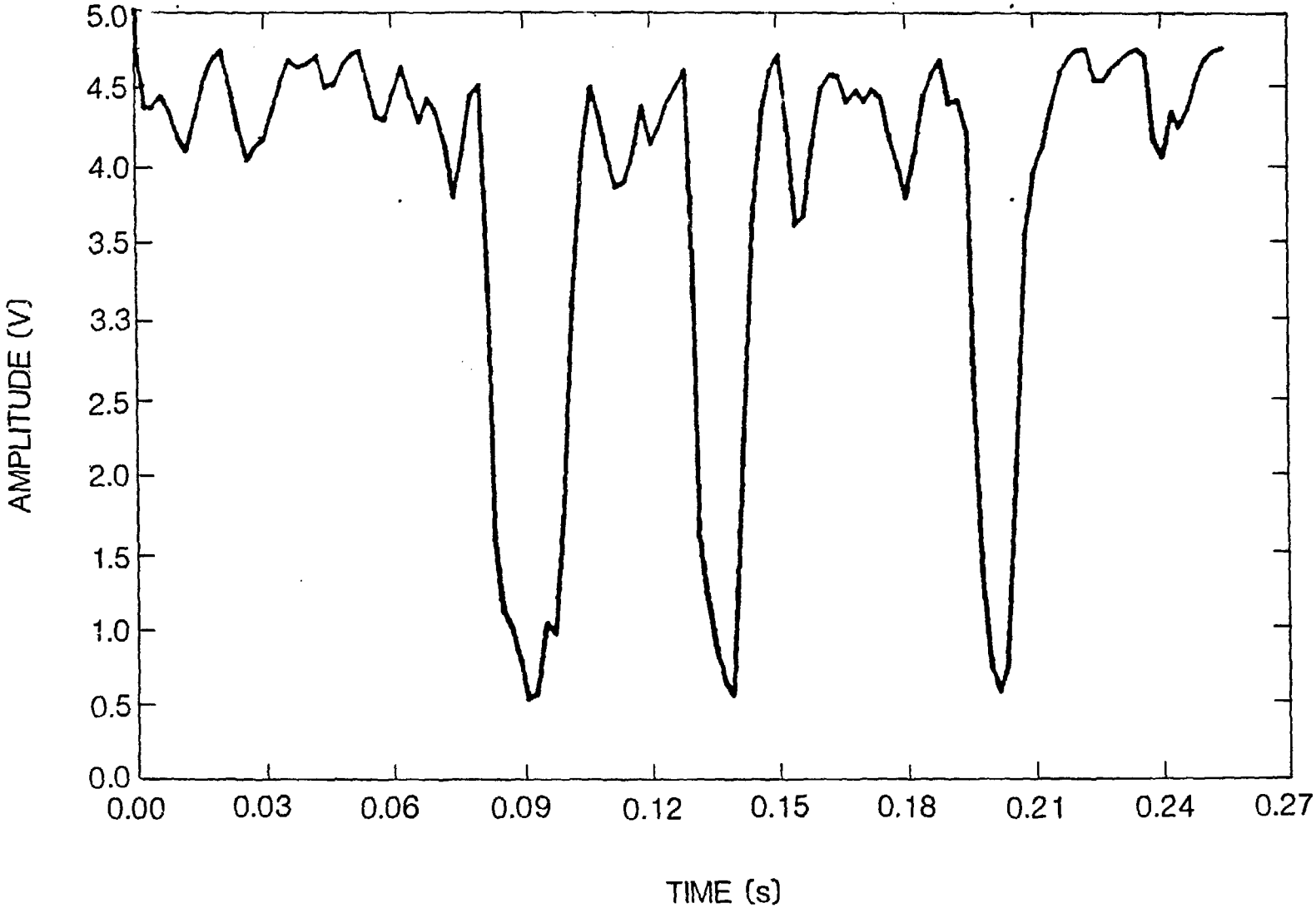

Fig. 2 An example of a simulated impedance probe signal.

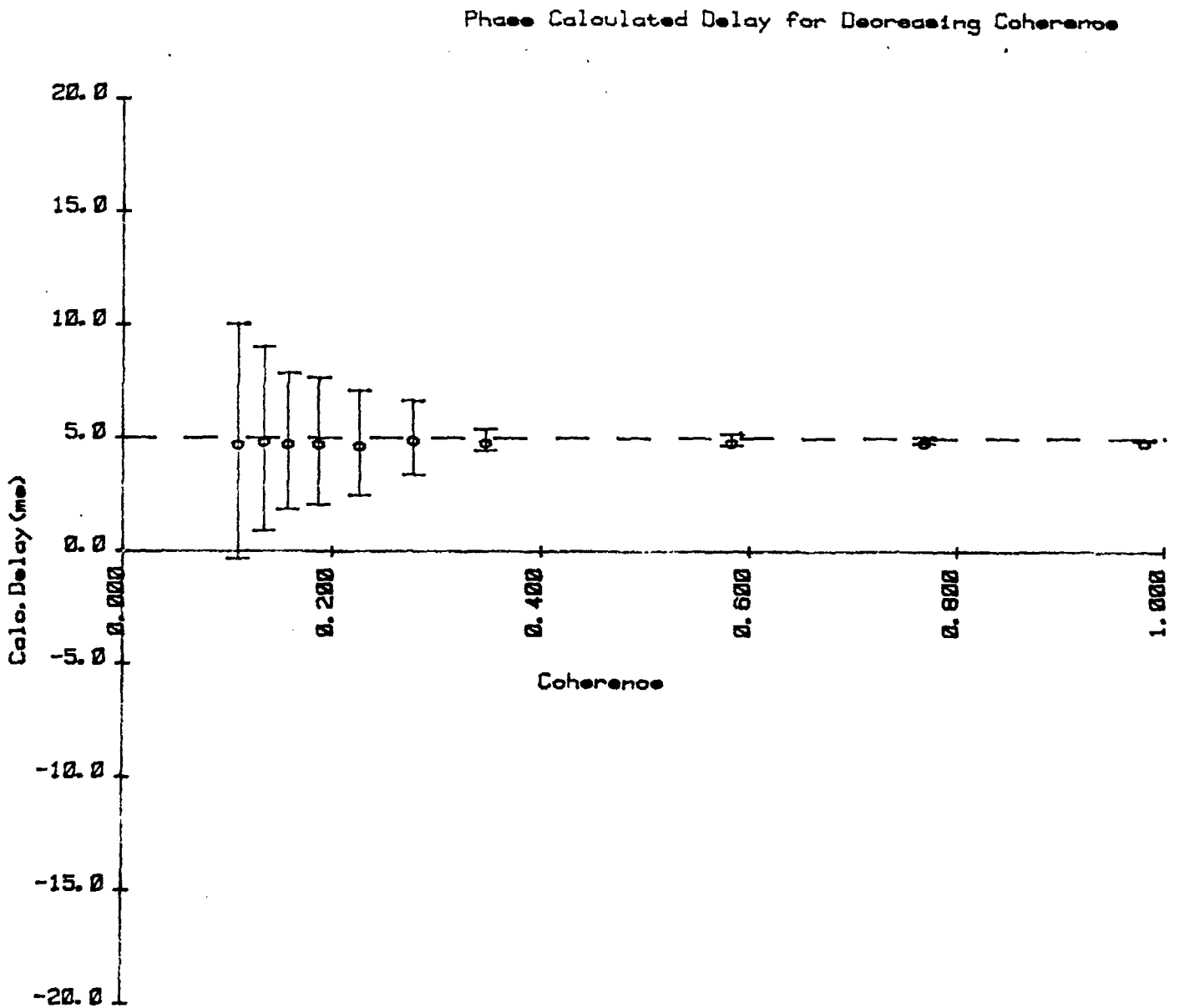

Fig. 3 Transit time as a function of coherence calculated with simulated signals having a delay of 5 ms.

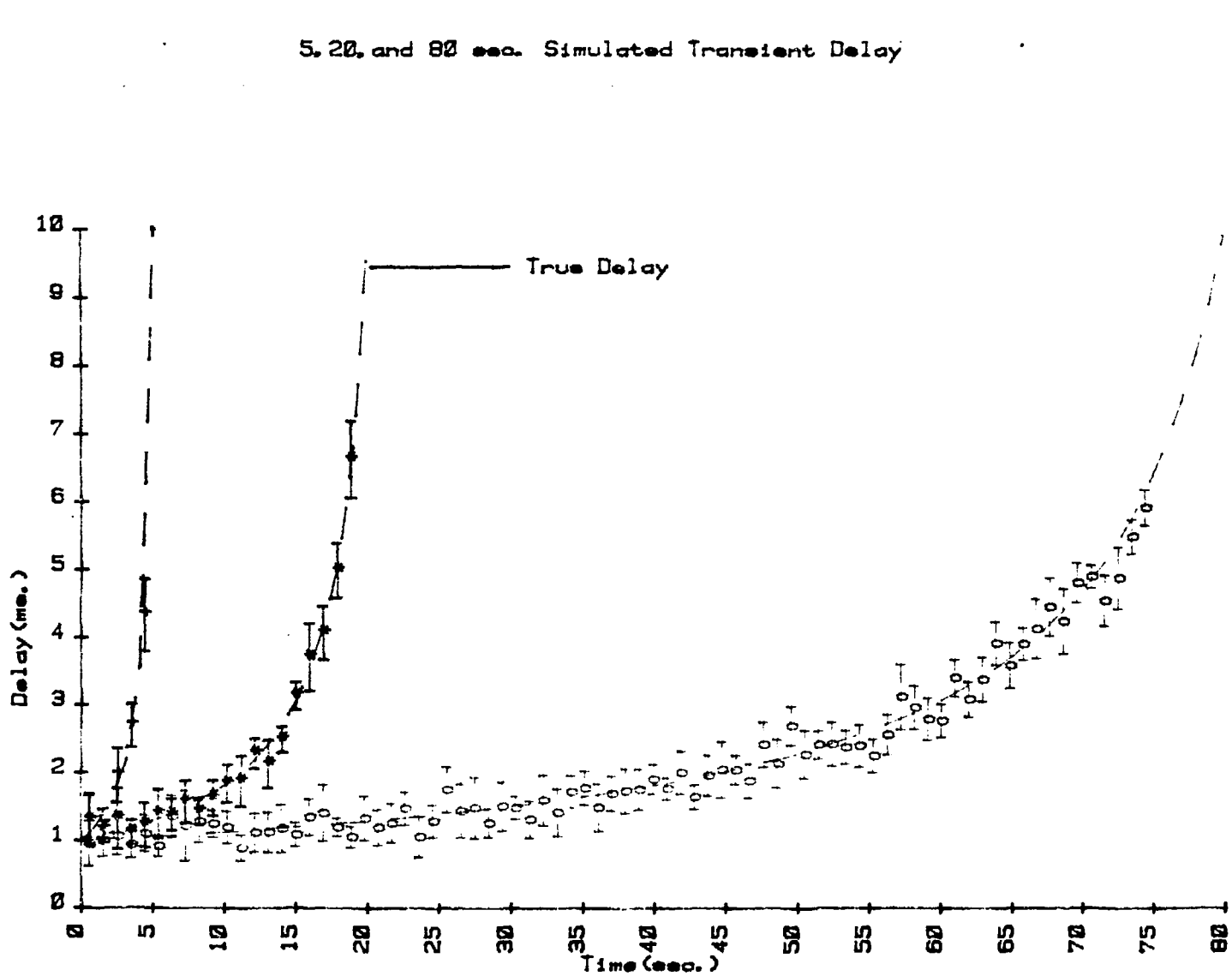

Fig. 4 Transit time versus time calculated for a 5, 20, and 80 s. simulated transient delay.

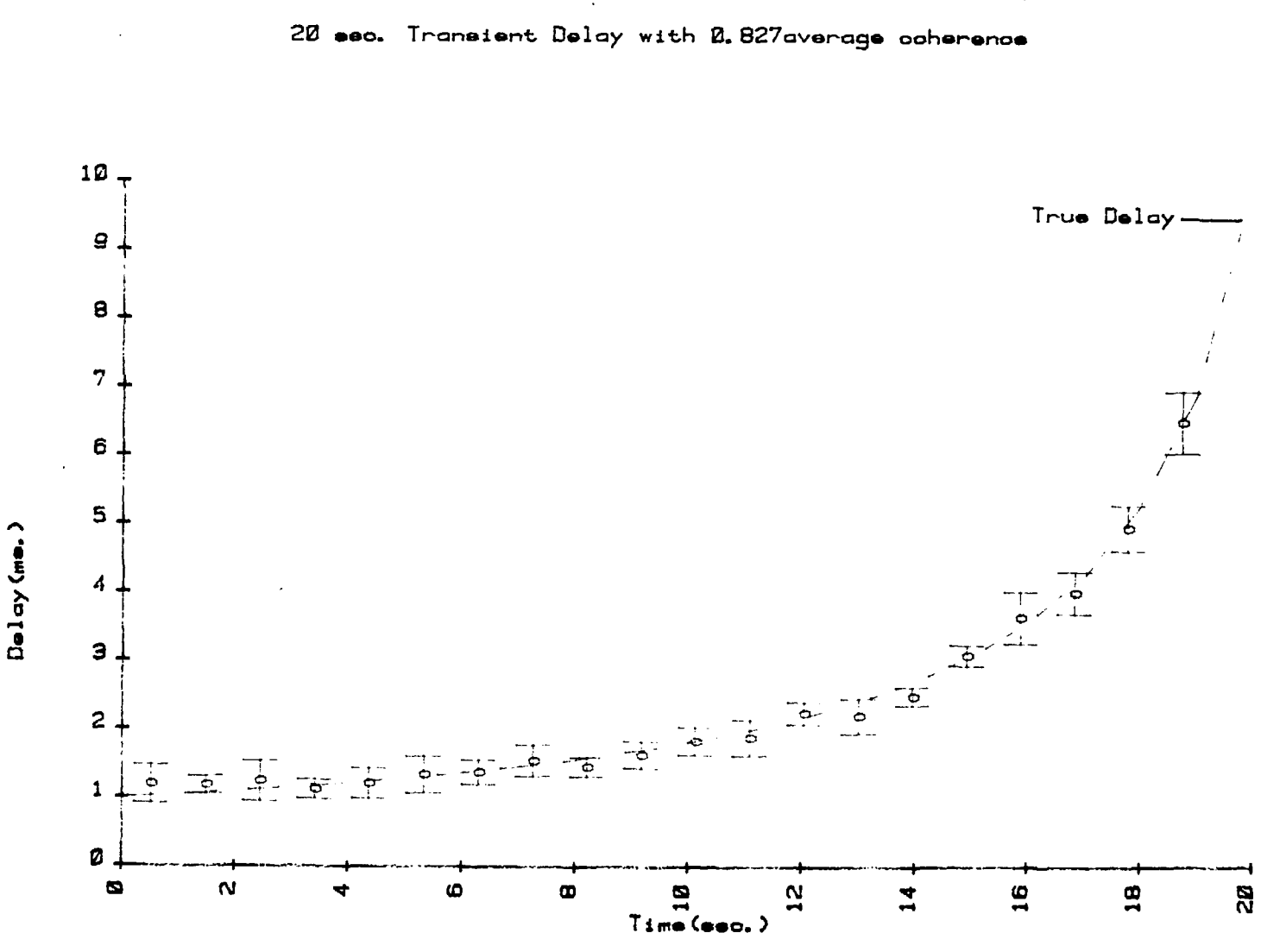

Fig. 5 Calculated transit time versus time for a 20 s simulated transient delay with a 0.8 average signal coherence.

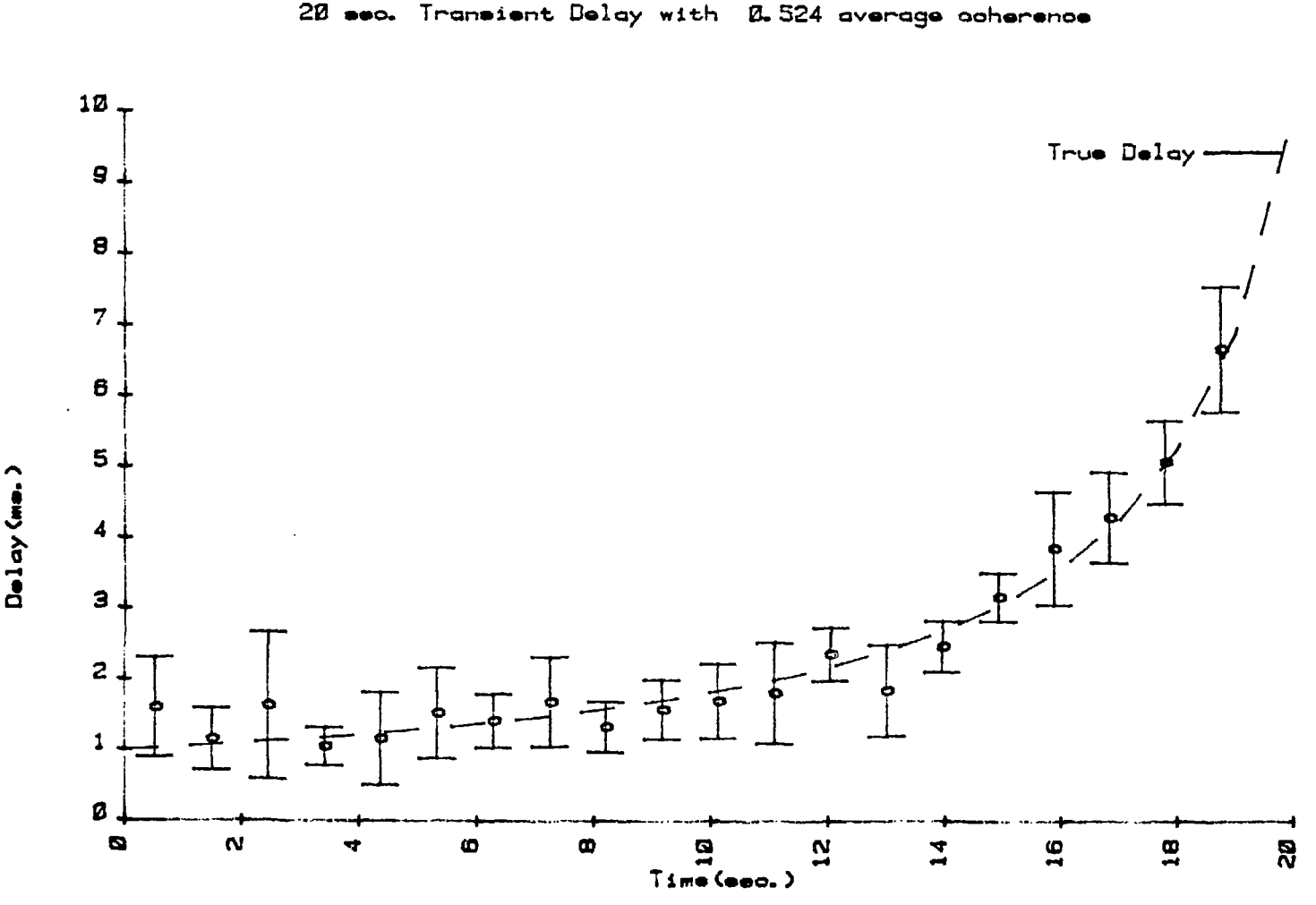

Fig. 6 Calculated transit time versus time for a 20 s simulated transient delay with a 0.5 average signal coherence.

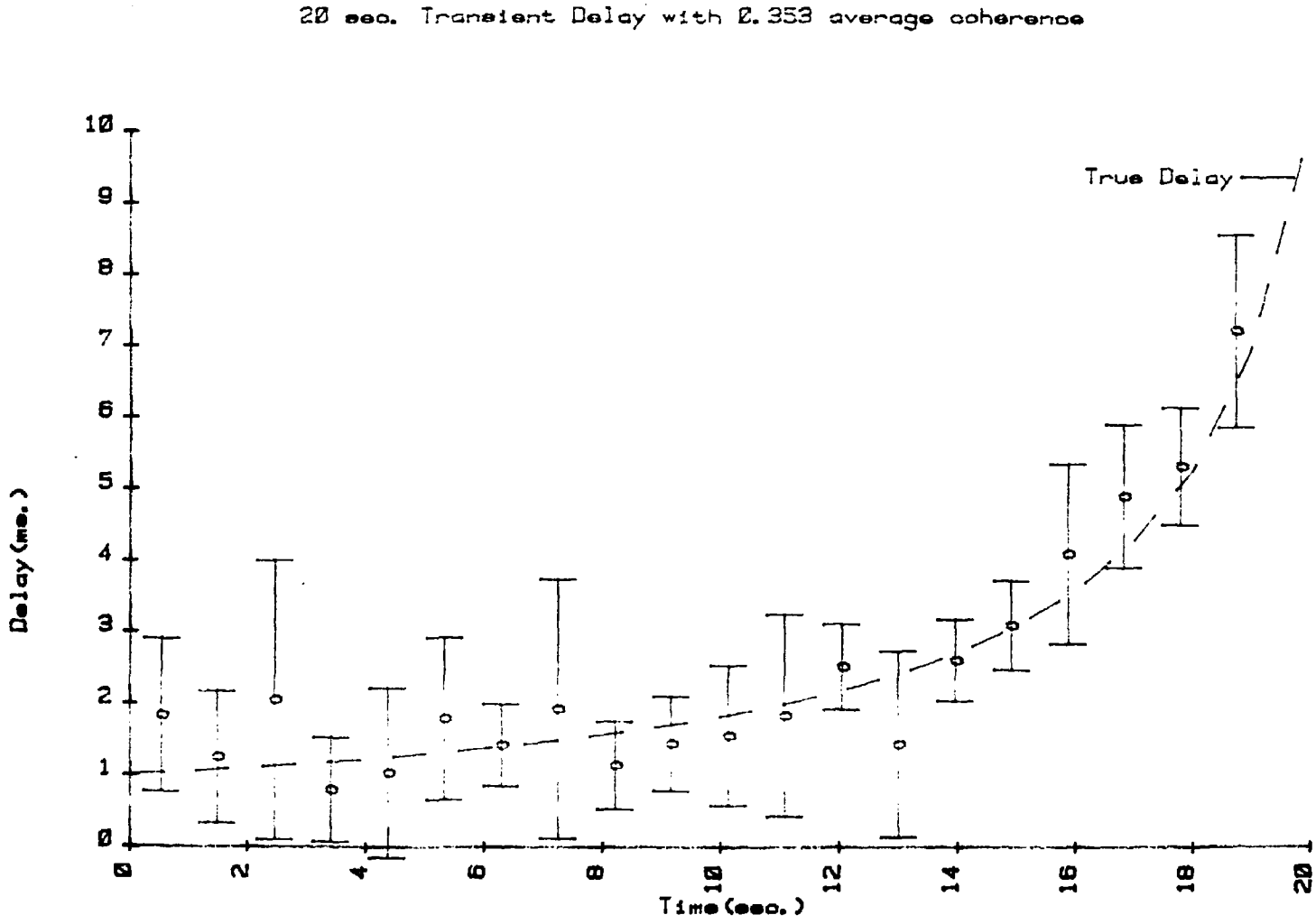

Fig. 7 Calculated transit time versus time for a 20 s simulated transient delay with a 0.3 average signal coherence.

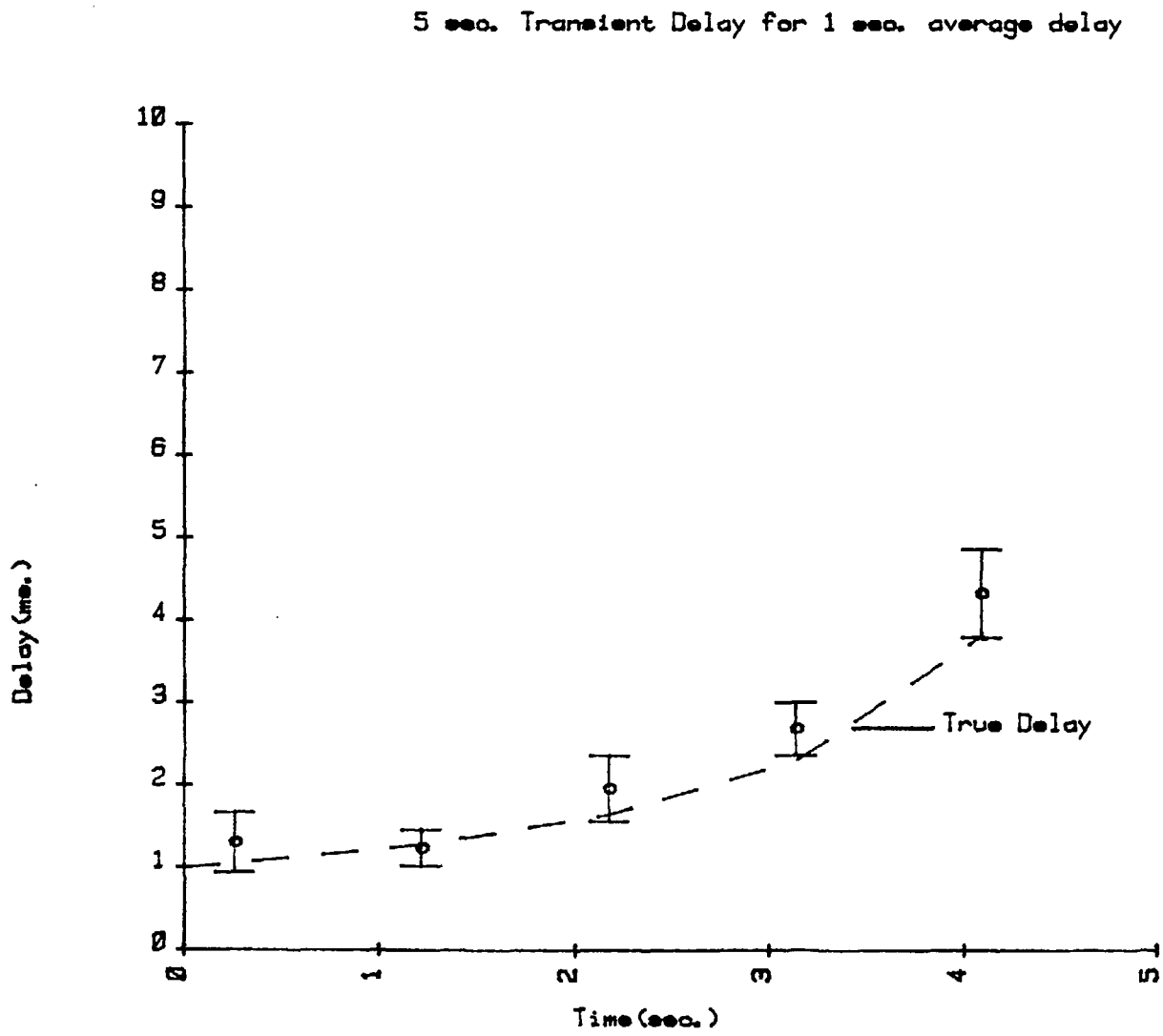

Fig. 8 1-s averaged transit time versus time for a 5 s simulated transient delay.

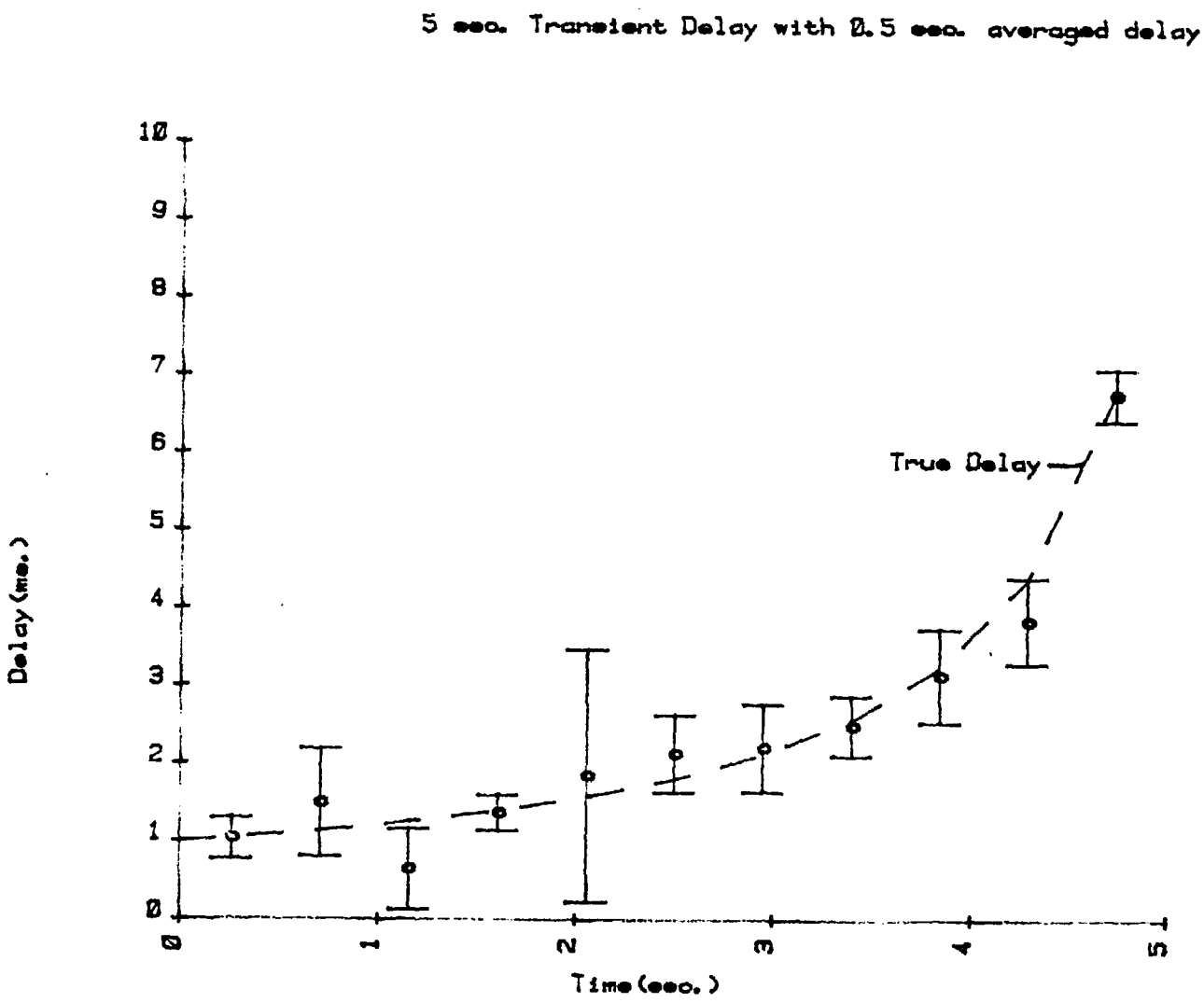

Fig. 9 0.5-s averaged transit time versus time for a 5 s simulated transient delay.

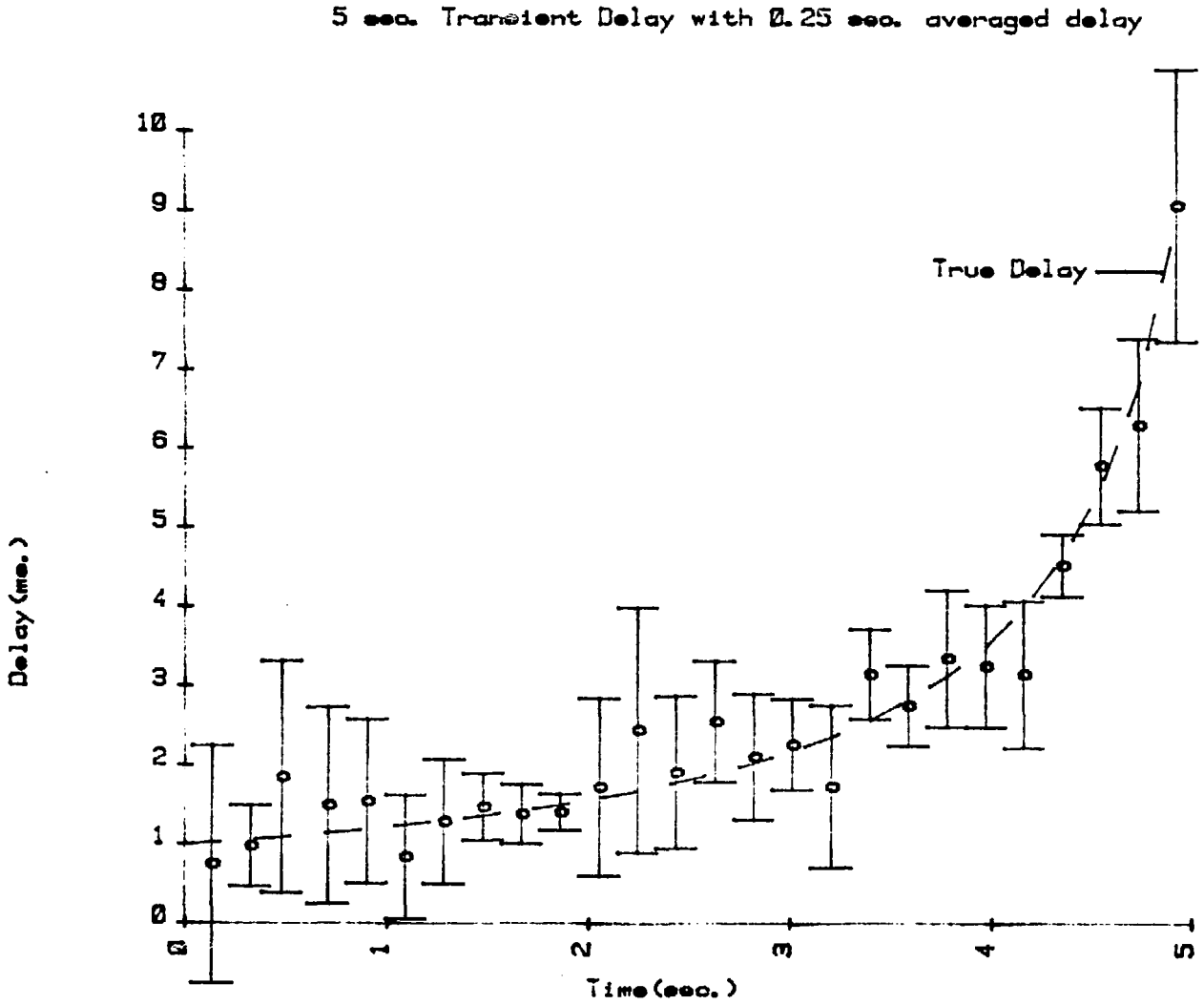

Fig. 10 0.25 averaged transit time versus time for a 5 s. simulated transient delay.

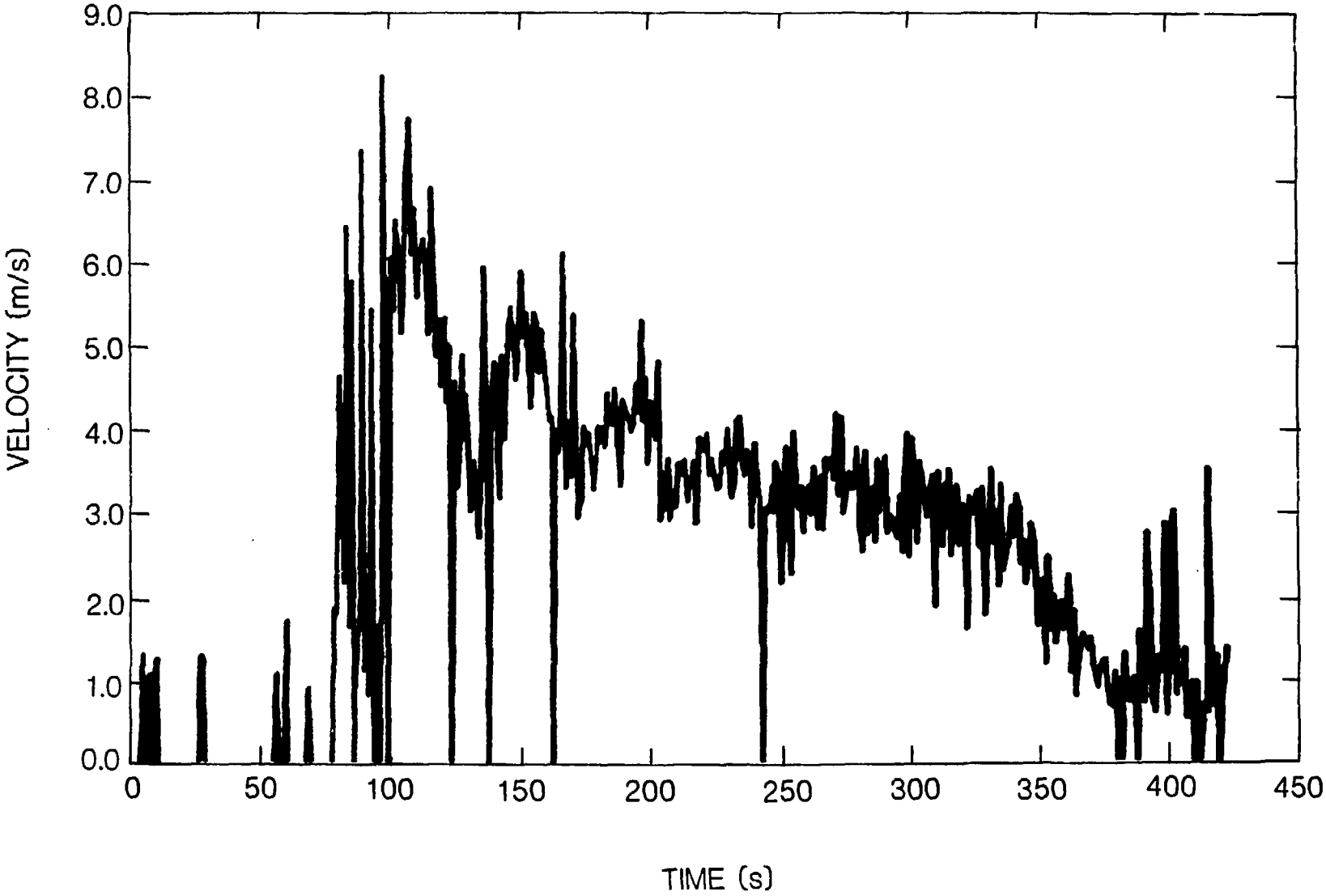

Fig. 11 Phase interface velocity versus time for a real steam-water transient produced by a simulated reflood experiment.

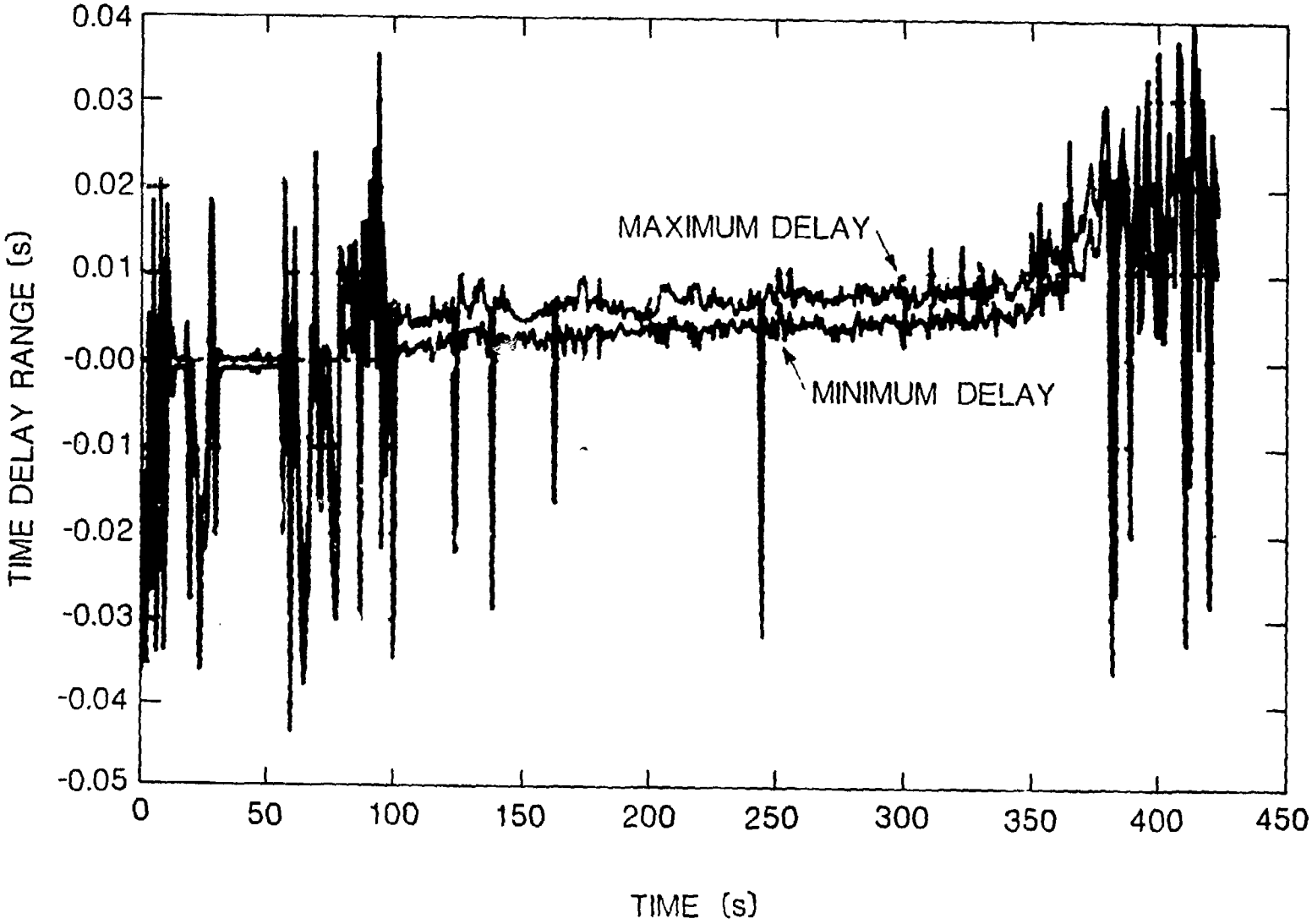

Fig. 12 Maximum and minimum transport delay calculated for a real steam-water transient produced by a simulated reflood experiment.

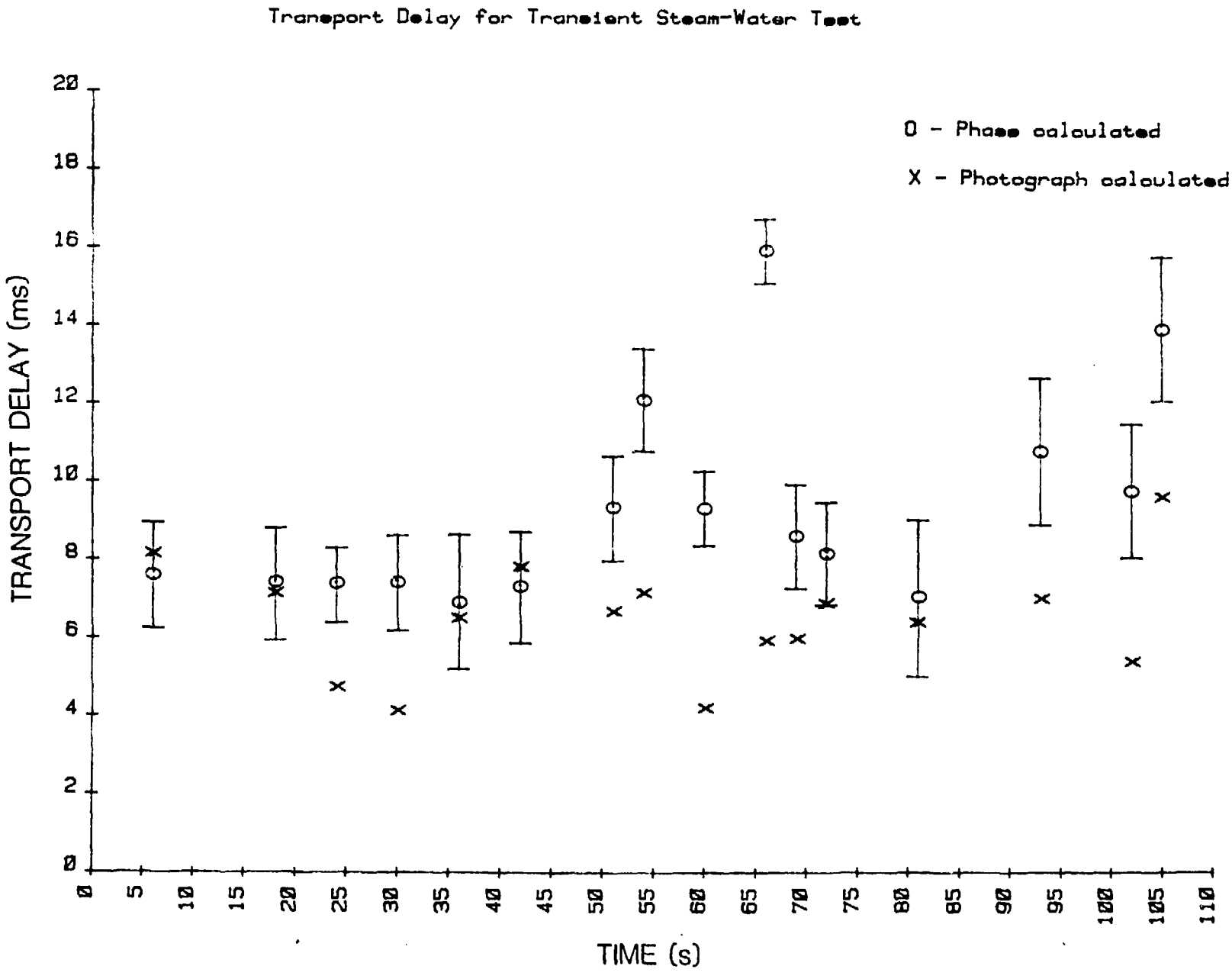

Fig. 13 A comparison versus time of transport delay calculated by the algorithm (0) and by high-speed photographs (x) for a part of